Title

3D MRI-based tumor delineation of ocular melanoma and its comparison with conventional techniques

Journal

Medical Physics, 32(11)

ISSN

0094-2405

Authors

Daftari, Inder K
Aghaian, E
O'Brien, J M
et al.

Publication Date

2005-11-01

Peer reviewed

3D MRI-based tumor delineation of ocular melanoma and its comparison with conventional techniques

Inder k Daftari[a)]
Department of Radiation Oncology, University of California, San Francisco, California 94143

Elsa Aghaian and Joan M. O'Brien
Ocular Oncology Unit, Department of Ophthalmology, University of California, San Francisco, California, 94143

William Dillon
Department of Radiology, University of California, San Francisco, California 94143

Theodore L. Phillips
Department of Radiation Oncology, University of California, San Francisco, California 94143

(Received 19 April 2005; revised 23 August 2005; accepted for publication 24 August 2005; published 18 October 2005)

The aim of this study is to (1) compare the delineation of the tumor volume for ocular melanoma on high-resolution three-dimensional (3D) T2-weighted fast spin echo magnetic resonance imaging (MRI) images with conventional techniques of A- and B-scan ultrasound, transcleral illumination, and placement of tantalum markers around tumor base and (2) to evaluate whether the surgically placed marker ring tumor delineation can be replaced by 3D MRI based tumor delineation. High-resolution 3D T2-weighted fast spin echo (3D FSE) MRI scans were obtained for 60 consecutive ocular melanoma patients using a 1.5 T MRI (GE Medical Systems, Milwaukee, WI), in a standard head coil. These patients were subsequently treated with proton beam therapy at the UC Davis Cyclotron, Davis, CA. The tumor was delineated by placement of tantalum rings (radio-opaque markers) around the tumor periphery as defined by pupillary transillumination during surgery. A point light source, placed against the sclera, was also used to confirm ring agreement with indirect ophthalmoscopy. When necessary, intraoperative ultrasound was also performed. The patients were planned using EYEPLAN software and the tumor volumes were obtained. For analysis, the tumors were divided into four categories based on tumor height and basal diameter. In order to assess the impact of high-resolution 3D T2 FSE MRI, the tumor volumes were outlined on the MRI scans by two independent observers and the tumor volumes calculated for each patient. Six (10%) of 60 patients had tumors, which were not visible on 3D MRI images. These six patients had tumors with tumor heights $\leqslant 3$ mm. A small intraobserver variation with a mean of $(-0.22 \pm 4)\%$ was seen in tumor volumes delineated by 3D T2 FSE MR images. The ratio of tumor volumes measured on MRI to EYEPLAN for the largest to the smallest tumor volumes varied between 0.993 and 1.02 for 54 patients. The tumor volumes measured directly on 3D T2 FSE MRI ranged from 4.03 to 0.075 $cm^{3.}$ with a mean of 0.87 ± 0.84 cm^3. The tumor shapes obtained from 3D T2 FSE MR images were comparable to the tumor shapes obtained using EYEPLAN software. The demonstration of intraocular tumor volumes with the high-resolution 3D fast spin echo T2 weighted MRI is excellent and provides additional information on tumor shape. We found a high degree of accuracy for tumor volumes with direct MRI volumetric measurements in uveal melanoma patients. In some patients with extra large tumors, the tumor base and shape was modified, because of the additional information obtained from 3D T2 FSE MR images. © *2005 American Association of Physicists in Medicine*. [DOI: 10.1118/1.2068927]

Key words: magnetic resonance imaging, uveal melanoma, proton therapy, tumor volume delineation

I. INTRODUCTION

Charged particle beams composed of protons or helium ions have a finite range in tissue, increased rate of energy loss near the end of range (Bragg-peak), sharp lateral penumbra, and deliver uniform dose to the target volume with an insignificant dose delivered to nearby structures. These properties are uniquely suited to precisely localize the radiation for treatment of orbital and eye tumors including many head and neck tumors.[1] Many centers around the world have used protons for the treatment of uveal melanoma.[2–12] For the best clinical results, careful attention must be applied to tumor localization, immobilization, treatment planning, and treatment verification.[13] Several authors[14–17] have calculated and measured the tumor volume in choroidal melanoma patients. These studies indicate that tumor volume is the best prognos-

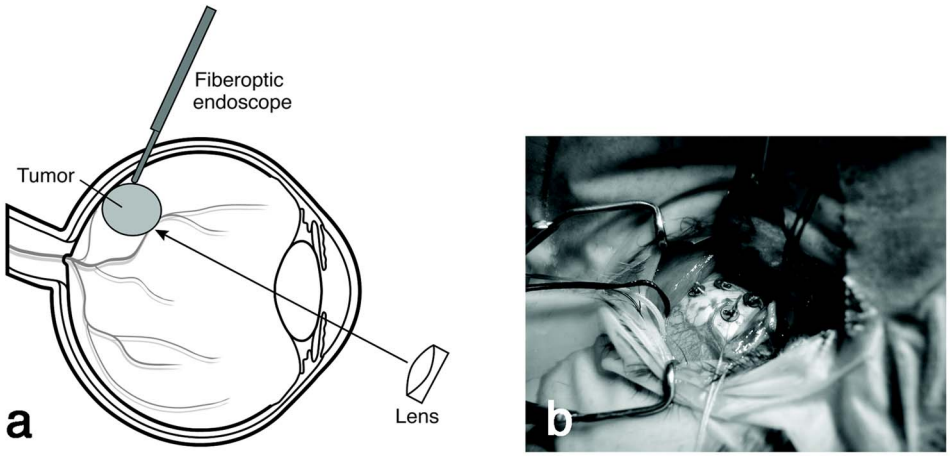

FIG. 1. (a) Indirect ophthalmoscopy and point source transillumination to delineate the tumor margins. (b) Tantalum rings 2.5 mm in diameter and 0.2 mm thick are sutured to the sclera to allow tumor localization during proton beam irradiation.

tic indicator for survival in choroidal melanoma patients followed by tumor basal diameter and tumor height.

Conventionally, the approach employed by ophthalmologists for diagnosis of uveal melanoma includes physical examination of the patients, laboratory tests, fluorescein angiography, A- and B-scan ultrasound, indirect ophthalmoscopy, slit lamp evaluation, and fundus photography. Transillumination and indirect ophthalmoscopy are used for tumor localization intraoperatively. Tantalum rings (radio-opaque markers 2.5 mm in diameter and 0.2 mm in thickness) are sutured surgically at four or five points on the sclera to outline the base of the tumor as shown in Fig. 1.

Indirect ophthalmoscopy with a transcleral point light source incorporated into an integrated fiber optic probe is used as an indentator on the outer sclera at our institution to confirm clip placement relative to tumor margins. This method to confirm accuracy of clip placement works very well and provides additional data for treatment planning. A limitation to this technique is that, the presence of hemorrhage, or severe cataract in some patients may limit visualization of the retina by indirect ophthalmoscopy and could result in a less accurate delineation of tumor margins in some of the patients. Also, ciliary body tumors and tumors in the anterior segment of the eye are difficult to confirm by these techniques. For these tumors, intraoperative high frequency ultrasound is used to confirm tumor margins relative to marker clip placement.[18,19]

Magnetic resonance imaging (MRI) of pigmented uveal melanoma results in a characteristic signal resulting from the paramagnetic properties of melanin.[20,21] Some investigators[20,21] have suggested that MRI may be helpful in the diagnosis of difficult melanoma cases. MRI may be superior to traditional A- and B-scan ultrasound in visualizing tumor invasion of surrounding soft tissue. In addition MRI provides tumor images in the sagittal and coronal planes, allowing better three-dimensional representation of the tumor volumes. A disadvantage of traditional MRI of the orbit lies in its inferior spatial accuracy. Also, because of the presence of large amounts of fat within the orbit, the small size of the ocular tumors, poor contrast, and eye movement, artifacts can become problematic. Recently, high-resolution three-dimensional (3D) fast spin echo T2-weighted MR imaging has become available which offers superior resolution of intraocular and orbital structures as compared to conventional MRI.

The aim of the present study is to (1) evaluate the usefulness of 3D T2 fast spin echo (FSE) MRI images in delineating the tumor volume and compare that to conventional techniques and (2) to evaluate whether the surgically placed marker ring tumor delineation can be replaced by 3D MRI based tumor delineation. In this study we describe 60 cases of choroidal melanoma in which tumor was delineated by conventional methods and patients were treated with proton beam therapy at Crocker Nuclear Laboratory, University of California, Davis.[6] The tumor volumes were further delineated on 3D T2 weighted FSE MRI images. To evaluate the usefulness of 3D T2 FSE MRI, the tumor volumes, size, and shape of tumors obtained from 3D T2 FSE MRI delineation were compared with conventional proton planning techniques. The shape of the tumors were further compared to the images obtained from fundus photographs and from EYEPLAN software.

II. MATERIAL AND METHODS

A. Patient population

This study consisted of 60 patients including 30 male and 30 female, ranging in age from 18 to 87 years with a mean of 59 ± 17 years. Twenty six (43%) had tumor in the anterior location and thirty four (57%) patients had posteriorly located tumor. In all the patients' tantalum rings were sutured to the sclera surgically by one of the authors (J.O.B.) to delineate the tumor margins. All patients were evaluated at the University of California San Francisco Ocular Oncology unit. The patients were planned using EYEPLAN software and were subsequently treated with proton beam radiation. Tumors were divided into four categories based on size: small (tumor thickness < 3 mm and basal diameter < 10 mm); medium (tumor thickness between 3 and 5 mm and basal diameter $\leqslant 15$ mm); large (tumor thickness between 5 and 10 mm and basal diameter $\leqslant 20$ mm) and extra-large

TABLE I. Characteristics of patients examined with 3D T2 FSE MRI imaging between March 2003 and March 2005.

						Percentiles	
		Mean	Median	Minimum	Maximum	25%	75%
Patients (n)	60						
Age (years)		59±17	60	18	87	47	69.5
Gender							
Female	30						
Male	30						
Site							
Right eye	30						
Left eye	30						
Tumor height (mm)		6±3.4	4.9	1.5	15.8	3.4	8.3
Basal diameter (mm)		13.4±4.6	13.5	2	24	10.6	16.8
Volume (mm^3)		808±839	480	78	4015	232	1070
Distance tumor-optic disc (mm)		4.7±6.4	1	0	21.4	0	7.0
Distance tumor-macula (mm)		4.5±6.2	1.6	0	21.1	0	7.2
Tumor size							
Small	7						
Medium	22						
Large	22						
X-large	9						
Tumor location							
Anterior	26						
Posterior	34						

(tumor thickness $\geqslant$ 10 mm or basal diameter $>$ 20 mm). The characteristics of the patients are provided in Table I.

B. Treatment planning

A computerized treatment-planning program "EYEPLAN" was used for all the patients treated with proton beam irradiation. This planning software was first developed by Goitein and Miller[23] and later modified at Clatterbridge, UK[24] and has been described in a previous publication.[25] The planning software uses information from the spatial coordinates of the tantalum marker rings relative to the axis of the eye, obtained from orthogonal x rays at the time of simulation. Axial diameter and tumor height measured by ultrasonography prior to treatment are also input to the planning program. The shape of the tumor is drawn manually on the computer screen using information from fundus drawings, fundus photography, ultrasound, fluorescein angiography, and the relation of tantalum rings to tumor margins described at the time of surgery by a map generated by the treating ophthalmologist. The aim of the treatment planning process is to select the optimal gaze angle, to design the shape of the field-defined aperture, and to determine the depth penetration of the beam and the width of the spread-out-Bragg peak necessary to encompass the target volume, and to determine the dose that each critical ocular structure will receive.

The tumor volumes[26] were calculated from the information of tumor length (l), width (w), tumor height (h_t) and the radius of the eye (R). The eye diameter and tumor height were obtained from ultrasound measurements. Tumor length and width were obtained from treatment planning. The tumor volume is assumed to consist of a paraboloid atop a circular base as shown in Fig. 2. Since the tumor grows inwardly, the total tumor volume (V_T) can be approximated by the addition of parabolic portion (V_p) plus spherical portion (V_s) (sitting above the circular base).

$$V_T = V_p + V_s, \tag{1}$$

where

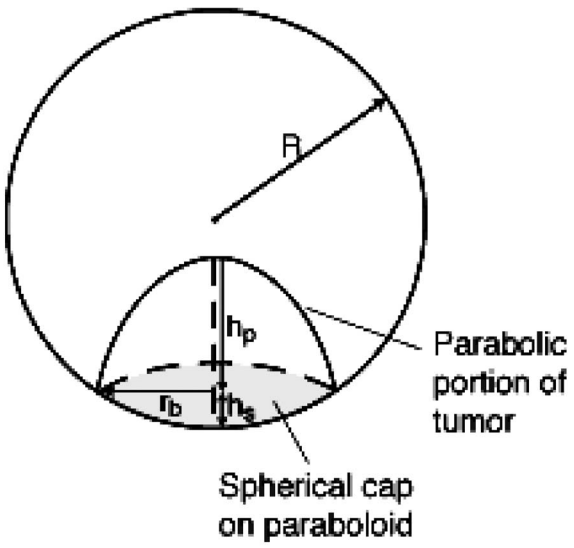

FIG. 2. Calculation of tumor volume based on spherical model.

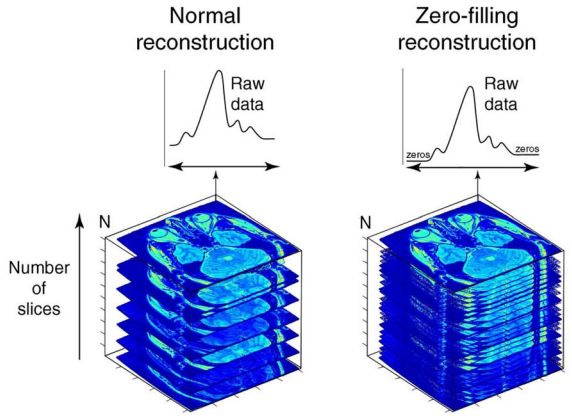

FIG. 3. Shows the schematics of the reconstruction of 3D T2 fast spin echo imaging. The zero filling reconstruction occurs before the inverse digital Fourier transform, which separates the volume signal into individual slices. The interpolation between the slices is caused by the zero filling such that the resulting image locations overlap each other. This figure was generated by reading individual MRI slices into image processing software tool of MATLAB (Ref. 28) and creating the 3D image.

$$V_p = \frac{\pi}{2} r_b^2 h_p \tag{2}$$

and

$$V_s = \pi/3 h_s^2 (3R - h_s). \tag{3}$$

R is the radius of the eye, $r_b = \sqrt{lw/\pi}$ radius of the circular base, $h_s = R - \sqrt{R^2 - r_b^2}$ height of spherical cap, and $h_p = h_t - h_s$ height of paraboloid.

C. Image acquisition and processing:

We used 3D T2-weighted fast spin echo MRI imaging (3D T2 FSE MRI) techniques to evaluate tumor delineation and its impact on treatment planning of ocular melanoma patients. This software produces contiguous thin sections for high quality multiplanar reconstruction. The technique, as described by Simon *et al.*,[22] employs a zero-filled slice interpolation method during postprocessing to further improve spatial resolution. Figure 3 provides a schematic of the 3D fast spin echo image reconstruction. The zero-filling reconstruction occurs before the inverse digital Fourier transformation, which separates the volume signal into individual slices. The interpolation between the slices is caused by the zero filling, such that the resulting image locations overlap each other. 3D T2-weighted FSE MRI imaging was obtained on all patients on a 1.5 T clinical system (General Electric, Milwaukee, WI) using a standard head coil. The system includes DICOM data communications. The following parameters were used to obtain images: 3000/102 (repetition time ms/echo time ms); field of view: 18 cm, matrix: 256×256, one excitation; fat suppression was used. The 3D MRI slices with 1.2–1.6 mm slice thickness, and 0.4 mm skip were acquired. This resulted in an in-plane resolution of 0.703 mm in the frequency-encoding direction and 0.938 mm in the phase-encoding direction. The coverage was typically 80 slices, which on the average took 10 min. The radiation oncologist, ocular oncologist, and neuroradiologist used 3D T2-weighted FSE MR images to define the tumor volumes. The data was transferred to a Power Mac G4 computer. The gross tumor volume was contoured on axial slices of 3D FSE MR images by two independent observers, a radiation oncologist and an ocular oncologist with help from neuroradiologist, which took on average 20 min on each patient. IMAGE J software[27] was used to contour and display images. IMAGE J is public-domain image processing software and can run on any platform with a Java Virtual Machine (Macintosh, Windows, and Unix), available from NIH, Bethesda, Maryland. This software has open architecture that allows addition of Java plug-ins. MATLAB[28] image processing tool kit was used to read the tumor contours and construct the tumor surface in three dimensions for comparison with EYEPLAN.

D. Volume definition

The target volume is generally defined by stacking 2D contours [i.e., region-of-interest (ROI's) with a thickness equal to the slice]. The target volume can be calculated using the following equation:

$$V = \sum_{s=1}^{N} (A_s \times T_s), \tag{4}$$

where N is the number of slices taken into account, T_s is the slice thickness, and A_s is the surface area of the ROI that defines the target volume on the slice S.

III. RESULTS

3D T2 FSE MRI was successfully performed on all 60 patients. MR imaging was unable to detect the tumor in 6 (10%) patients. For these patients, the tumor height was $\leqslant 3$ mm when measured with ultrasound. Small melanomas were found in 7 (11.7%) patients; medium size melanomas in 36.7%; large melanomas in 36.7%, and extra-large tumors in 15% of patients. Dome-shaped tumors were found in 8 (13%) patients, tumors in the peripapillary location were found in 11 (18%) patients, and ciliary body melanoma in 12 (20%) patients. Flat or diffuse tumors were found in 4 (7%) patients and oval shape tumor in 2 (3%) patients. In 34 (57%) patients, the main portion of the tumor was located in the posterior pole of the eye, whereas in 26 (43%) patients, it was found in the anterior segment of the eye.

Interobserver reliability for delineating the tumor volumes was excellent. Figure 4 shows the frequency distribution of tumor volumes estimated by two observers and derived from EYEPLAN. The distribution is divided into two parts (a) for small and medium sized tumors and (b) for large and extra large tumors. As demonstrated in (Fig. 4), tumor volumes obtained by the two methods are very close. Since the difference in tumor volume estimates between observer 1 and observer 2 are small, we obtained the average tumor volume from observer 1 and 2. There was no significant difference in tumor volumes with different tumor shapes. The tumor volume difference varied between 6.3% and 1.1% for small size tumors, where EYEPLAN overestimated the tumor volume by

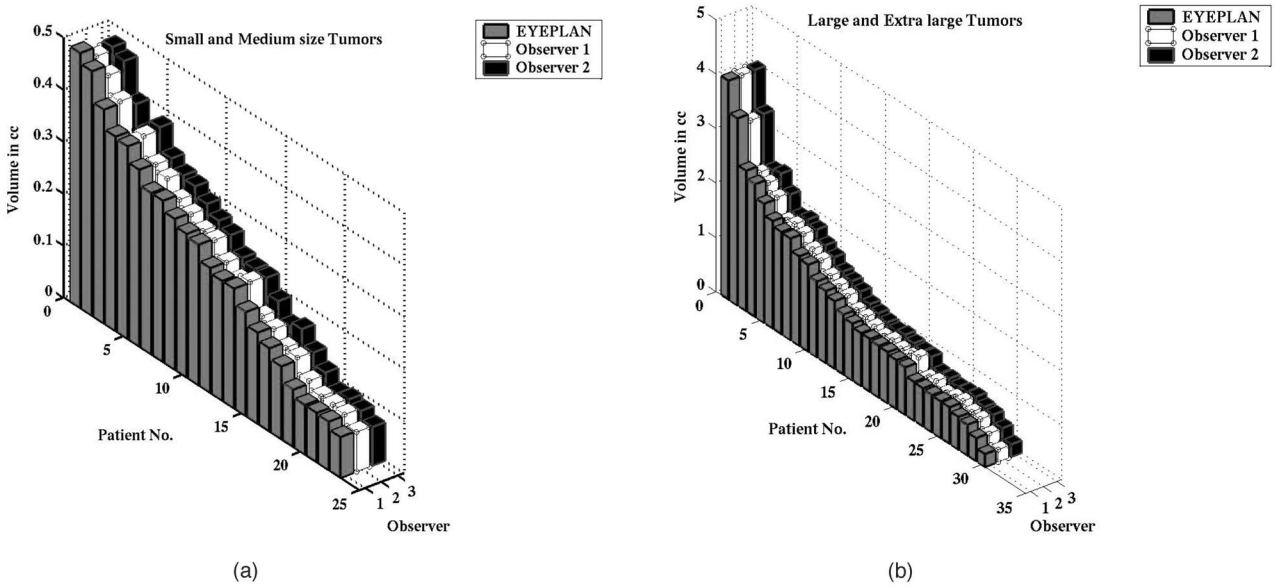

FIG. 4. The tumor volume identified by two observers (physicians) in comparison to the tumor volume obtained from EYEPLAN software. (a) For small and medium size tumors and (b) large and extra-large tumors. The differences among tumor volumes in comparison to EYEPLAN tumor volume were minimum.

6% for two patients as compared to tumor volumes estimated by 3D T2 MRI images. It varied from −4.1% to 5% for medium size, from −5.7% to 6.2% for large tumors, and from −2.4% to 5.8% for extra-large tumors. The difference of 6% between tumor volumes obtained by conventional methods and tumor volumes obtained from 3D T2 FSE MR images represents either an overestimate of tumor by conventional approaches or an error in 3D T2 FSE images defining the tumor contours. The ratio of tumor volumes as obtained from 3D MRI to EYEPLAN for the largest to the smallest tumor volumes varied between 0.993 and 1.02 for 54 patients. Table II summarizes the interobserver variability for delineation of tumor volume on 3D T2 FSE MRI scans as expressed using coefficients of variance (COV) defined below.

$$\text{COV} = (\text{standard deviation of all measurements per observer/arithmetic mean}) \times 100.$$

No statistically significant difference greater than zero was present in interobserver variability between observers as compared to EYEPLAN (paired t test).

Figure 5 provides several different approaches to imaging a patient with a uveal melanoma of the choroid involving the pars plana at 9:00. Figures 5(a) and 5(b) provide traditional A- and B-scan ultrasound images of this tumor. On A scan, there is a typical pattern for uveal melanoma, which exhibits spontaneous pulsations, low to moderate reflectivity, and a relatively sharp posterior spike. Figure 5(b) is a B-scan image of this dome shaped tumor arising from the choroid with associated subretinal fluid. Figure 5(c) is a transverse slice of 3D T2 FSE MR image, which clearly defines the tumor and its shape. This shape of the choroidal mass on 3D FSE image is similar to the shape of the tumor defined by fundus photography [Fig. 5(d)]. The tumor drawn in the treatment planning program [Fig. 5(e)] matches with the shape from MRI images and fundus photography. It also matched in lateral view from EYEPLAN software to sagittal view from MRI (not shown here). The tumor contours drawn on 3D MRI slices are stacked, representing the 3D surface of the tumor [Fig. 5(f)]. Figure 5 suggests that 3D T2 FSE MRI imaging provides complimentary information to confirm the tumors basal dimensions and its unique configuration in space. This has shown that 3D MRI tumor delineation is as good as marker base tumor delineation. The impact of 3D T2 FSE MRI imaging was to modify the tumor base in two patients with extra large tumors. Due to the large tumor thickness more

TABLE II. Intraobserver coefficient of variance calculated for each observer and for EYEPLAN. The results are not statistically significant between both methods of estimation.

		Tumor volume (cm^3)				
Planner	Observations	Mean	SD	Ratio	COV (%)	p value
Observer 1	54	0.874	0.844	0.995±.04	96.7	0.14
Observer 2	54	0.869	0.840	0.994±.03	96.7	0.02
EYEPLAN	54	0.879	0.855	1.00	97.3	

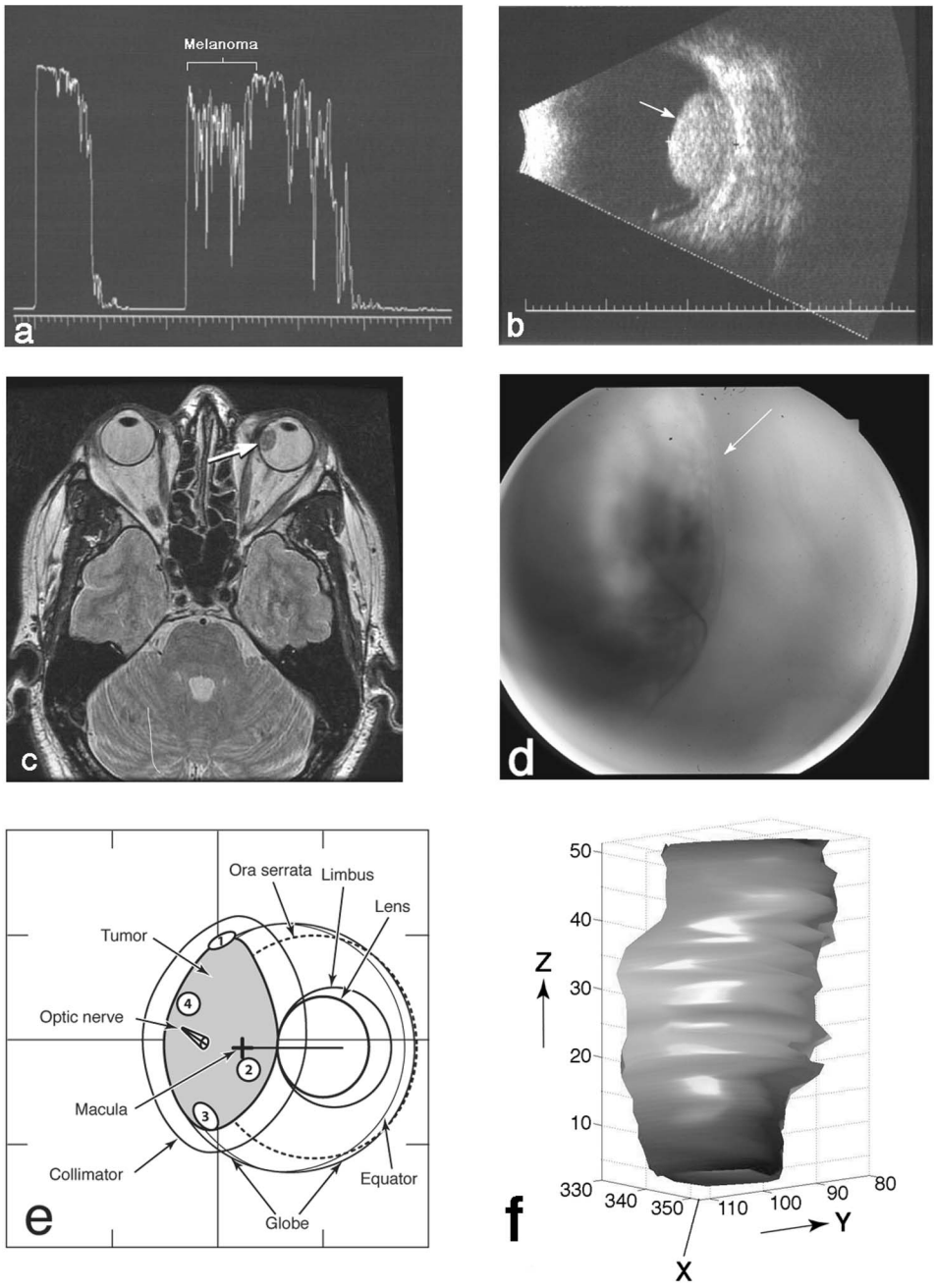

FIG. 5. Illustrates an example of uveal melanoma of the choroid. (a) The A-scan ultra sonogram showing a typical pattern of a uveal melanoma, which exhibits spontaneous pulsations, low to moderate reflectivity, and a relatively sharp posterior spike. (b) The B scan, demonstrates a tumor (arrow) showing marked growth of the lesion to 8.3 mm in anterior-to-posterior height. (c) Axial 3D T2-weighted FSE MRI slices showing the dome shaped tumor in the left eye. (d) Shows the fundus view of the same lesion. (e) Illustrates the treatment plan in the beam's eye view of the lesion using polar and azumith angle of (25°,0°). Various structures in the model are labeled. The contour around the tumor represents the 50% isodose line. (f) The tumor surface generated by stacking the tumor contours on sequential MRI slices using MATLAB image processing system.

than 10 mm, the tumor was overhanging the optic nerve. It was very difficult to see the base of the tumor with transillumination. 3D T2 FSE MRI images clearly showed the tumor margin from the optic nerve. In one patient, the tumor thickness was overestimated by ultrasound measurement. The measurement of tumor thickness was about 3 mm less as obtained from 3D T2 FSE MRI images, which made a difference in treatment planning.

IV. DISCUSSION

The diagnosis, treatment planning and evaluation of a particular therapy is often supported by various imaging modalities. For example, magnetic resonance imaging, computer tomography, and ultrasound imaging depict the aspects of anatomy, which compliment the treatment planning process. In many instances it is desirable to integrate the information from different imaging modalities for the same patient as is often done in conventional radiation therapy. Several studies[20,29,30] have described different features of magnetic resonance imaging of orbital tumors. MRI imaging differentiates pigmented uveal melanoma from other simulating lesions. However, MRI has a disadvantage which lies in its partial volume effect that occurs at the intersection of several structures within one or the same pixel. The error due to the partial volume effect is dependent on the pixel size and the slice thickness. Thus, increasing resolution and reducing the slice thickness is going to reduce the partial volume effect. For several patients, we delineated the tumor on 3D T2 FSE

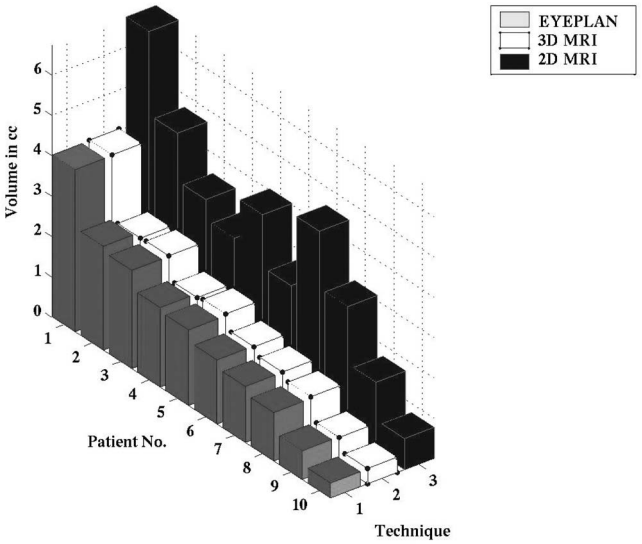

FIG. 6. Tumor volume measured for different patients using EYEPLAN, 3D MRI, and 2D MRI techniques.

MRI scans as well as on conventional axial MRI scans with slice thickness of 3 mm and interslice space of 3 mm. It was observed that the volume of tumor was overestimated on conventional MRI scans as compared to 3D T2 FSE MRI as is noted from Fig. 6. Caudrelier *et al.*[31] calculated the target volumes on MRI scans by classical and fuzzy logic methods. They observed that the volumes calculated by classical methods increase quasiexponentially as the MRI slice thickness increases. McCaffery *et al.*[32] clinically evaluated three-dimensional fast spin echo T2-weighted imaging techniques for orbital tumors. They concluded that this newer approach to MRI imaging improved diagnostic accuracy of orbital and intraocular malignancies. No study to date has evaluated the utility of 3D FSE T2-weighted MRI imaging to improve treatment planning for an intraocular malignancy, uveal melanoma.

Our observations in these 60 cases suggest that 3D T2-weighted fast spin echo MRI is useful not only for the diagnosis of choroidal melanoma but also for treatment planning. 3D T2 FSE MRI detected 54 uveal melanomas out of 60 patients evaluated. The size of the undetected tumors was small to medium with tumor height $\leqslant 3$ mm. Promising results were obtained with respect to the delineation of tumor volume. Findings were similar for observers 1 and 2, a difference of -9 to 13 % in volume estimation was obtained between observers 1 and 2 with a mean of -0.22 ± 4 %. The volumetric data estimation shows sufficient agreement between EYEPLAN and 3D T2 FSE MRI imaging. A difference of $\pm 6\%$ was observed between the two methods. There is also an element of human error in manually drawing the tumor volumes on MRI slices and in manually drawing the tumor volume on the computer screen using EYEPLAN treatment planning software. The fact that tumor shapes obtained from the 3D T2 FSE MRI imaging were comparable to the shapes obtained from fundus photography and from treatment planning provides additional confidence in irradiating these patients. MRI imaging was particularly helpful in delineating tumor margin in patients where tumor was surrounded by hemorrhage or dark reactive pigmentation. It was helpful in modifying the tumor base with extra large tumors. In one patient the tumor thickness was overestimated by ultrasound as compared to 3D T2 FSE MRI images. It is our impression that tumor volumes measured on 3D MRI images are repeatable, reliable, and can be generated easily, having great potential for use in the diagnosis and treatment of malignant intraocular tumors. One possible use of 3D T2 FSE MRI may be in delineating and treating many choroidal melanomas and choroidal metastases without implanting tantalum markers. Recently, we treated two patients with choroidal metastases with radiosurgical methods using "CyberKnife" (Accuray Inc., Sunnyvale, CA) without implanting tantalum markers[33] using noninvasive methods for eye fixation. However, the use of 3D T2 FSE MRI imaging for delineation of tumor and eventually doing the treatment without the tantalum rings should be further investigated. We are planning on doing this first with patients who have choroidal metastases in a Committee of Human Research (CHR) approved phase II study. Eventual use in choroidal melanoma using protons as well as radiosurgical techniques will depend on noninvasive eye fixation and monitoring. A preliminary study of three radiosurgical techniques suggests that coverage and normal tissue sparing could be comparable to proton beam therapy.[34] Thus this 3D MRI method of tumor delineation should lead to exciting future research.

V. CONCLUSION

This is the first study to evaluate 3D T2-weighted fast spin echo MR images for delineation of tumor (uveal melanoma) volumes and to compare these tumor volumes to volumes obtained from the treatment planning program "EYEPLAN." The comparison of tumor volumes and tumor shapes show promising and interesting results. 3D FSE MRI imaging will become a valuable tool to compliment more traditional approaches to the treatment planning of uveal melanoma patients for proton beam therapy and may allow the elimination of invasive marker placement in most patients.

ACKNOWLEDGMENTS

This study was supported in part by Knights Templar Eye Foundation, Inc., Chicago, IL, Fight For Sight, Inc., New York, NY, and R01 Department of Ophthalmology core Grant No. EY02162, National Eye Institute, Bethesda, MD. The authors are thankful to Dr. Lynn Verhey for his critical reading of the manuscript and his valuable suggestions.

[a]Electronic mail: Daftari@radonc17.ucsf.edu

[1]J. R. Castro, "Results of heavy ion radiotherapy," Radiat. Environ. Biophys. **4**, 45–48 (1995).
[2]D. E. Bonnett, A. Kacperek, M. A. Sheen, R. Goodall, and T. E. Saxton, "The 62 MeV Proton-Beam for the Treatment of Ocular Melanoma at Clatterbridge," Br. J. Radiol. **66**, 907–914 (1993).
[3]G. Cuttone, A. Amato, A. Bartolotta, M. Brai, G. A. P. Cirrone, A. Giammo, S. Lo Nigro, G. A. Nicoletti, J. Ott, G. Privitera, L. Raffaele, M.

L. Rallo, C. Rapicavoli, A. Reibaldi, D. Rifuggiato, N. Romeo, A. Rovelli, M. G. Sabini, V. Salamone, G. Teri, and F. Tudisco, "Use of 62 MeV proton beam for medical applications at INFN-LNS: CATANA project," Phys. Medica **17**, 23–25 (2001).
[4]S. Hocht, N. E. Bechrakis, M. Nausner, K. Kreusel, H. Kluge, J. Heese, J. Heufelder, D. Cordini, H. Homeyer, H. Fuchs, P. Martus, M. H. Foerster, T. Wiegel, and W. Hinkelbein, "Proton Therapy of Uveal Melanomas in Berlin," Strahlenther. Onkol. **180**, 419–424 (2004).
[5]M. Fuss, L. N. Loredo, P. A. Blacharski, R. I. Grove, and J. D. Slater, "Proton radiation therapy for medium and large choroidal melanoma: Preservation of the eye and its functionality," Int. J. Radiat. Oncol., Biol., Phys. **49**, 1053–1059 (2001).
[6]I. K. Daftari, T. R. Renner, L. J. Verhey, R. P. Singh, M. A. Nyman, P. L. Petti, and J. R. Castro, "New UCSF proton ocular beam facility at the Crocker Nuclear Laboratory Cyclotron (UC Davis)," Nucl. Instrum. Methods Phys. Res. A **380**, 597–612 (1996).
[7]C. Spatola, G. Privitera, L. Raffaele, V. Salamone, G. Cuttone, P. Cirrone, M. G. Sabini, and S. Lo Nigro, "Clinical application of proton beams in the treatment of uveal melanoma: The first therapies carried out in Italy and preliminary results (Catana project)," Tumori **89**, 502–509 (2003).
[8]P. Chauvel, N. Brassart, J. Herault, and A. Courdi, "Nice proton therapy center," Pathol. Biol. (Paris) **41**, 126–128 (1993).
[9]P. Chauvel, A. Courdi, J. N. Bruneton, J. Caujolle, J. Grange, and L. Diallo-Rosier, "Proton therapy of uveal melanomas in Nice: A 6.5-year follow-up study," Radiology **209P**, 401–402 (1998).
[10]A. Courdi, J. P. Caujolle, J. D. Grange, L. Diallo-Rosier, J. Sahel, F. Bacin, C. Zur, P. Gastaud, N. Iborra-Brassart, J. Herault, and P. Chauvel, "Results of proton therapy of uveal melanomas treated in Nice," Int. J. Radiat. Oncol., Biol., Phys. **45**, 5–11 (1999).
[11]E. Egger, L. Zografos, A. Schalenbourg, D. Beati, T. Bohringer, L. Chamot, and G. Goitein, "Eye retention after proton beam radiotherapy for uveal melanoma," Int. J. Radiat. Oncol., Biol., Phys. **55**, 867–880 (2003).
[12]L. Lumbroso, C. Levy, C. Plancher, E. Frau, F. D'Hermies, P. Schlienger, R. Dendale, H. Mammar, S. Delacroix, C. Nauraye, G. Noel, R. Ferrand, C. Desblancs, A. Mazal, P. Validire, B. Asselain, and L. Desjardins, "Results of proton beam irradiation for treatment of choroidal melanoma," J. Fr. Ophtalmol **25**, 290–297 (2002).
[13]E. S. Gragoudas, K. M. Egan, J. M. Seddon, S. M. Walsh, and J. E. Munzenrider, "Intraocular recurrence of uveal melanoma after proton beam irradiation," Ophthalmology **99**, 760–766 (1992).
[14]D. H. Char, S. Kroll, and T. L. Phillips, "Uveal melanoma. growth rate and prognosis," Arch. Ophthalmol. (Chicago) **115**, 1014–1018 (1997).
[15]P. K. Jensen and M. K. Hansen, "Ultrasonographic, three dimensional scanning for determination of intraocular tumor volume," Acta Ophthalmol. **69**, 178–186 (1991).
[16]W. J. Li, E. S. Gragoudas, and K. M. Egan, "Tumor basal area and metastatic death after proton beam irradiation for choroidal melanoma," Arch. Ophthalmol. (Chicago) **121**, 68–72 (2003).
[17]E. Richtig, G. Langmann, K. Mullner, G. Richtig, and J. Smolle, "Calculated tumour volume as a prognostic parameter for survival in choroidal melanomas," Eye **18**, 619–623 (2004).
[18]I. Daftari, D. Barash, S. Lin, and J. O'Brien, "Use of high-frequency ultrasound imaging to improve delineation of anterior uveal melanoma for proton irradiation," Phys. Med. Biol. **46**, 579–590 (2001).
[19]P. R. Golchet, I. K. Daftari, S. Lin, V. Weinberg, and J. M. O'Brien, "Intra-operative ultrasound biomicroscopy in proton irradiation of anterior uveal melanoma," Invest. Ophthalmol. Visual Sci. **44**, U286–U286 (2003).
[20]R. G. Peyster, J. J. Augsburger, J. A. Shields, B. L. Hershey, R. Eagle, and M. E. Haskin, "Intraocular tumors: evaluation with MR imaging," Radiology **168**, 773–779 (1988).
[21]M. F. Mafee, G. A. Peyman, J. H. Peace, S. B. Cohen, and M. W. Mitchell, "Magnetic resonance imaging in the evaluation and differentiation of uveal melanoma," Ophthalmology **94**, 341–348 (1987).
[22]E. M. Simon, S. McCaffery, H. A. Rowley, N. J. Fischbein, A. Shimikawa, and J. M. O'Brien, "High-resolution 3D T2-weighted fast spin echo: New applications in the orbit," Neuroradiology **45**, 489–492 (2003).
[23]M. Goitein and T. Miller, "Planning proton therapy of the eye," Med. Phys. **10**, 275–283 (1983).
[24]M. A. Sheen, in *20th PTCOG Meeting*, 1994, Vol. 29 (Chester, England, 1994) pp. 16–18.
[25]I. K. Daftari, D. H. Char, L. J. Verhey, J. R. Castro, P. L. Petti, W. J. Meecham, S. Kroll, and E. A. Blakely, "Anterior segment sparing to reduce charged particle radiotherapy complications in uveal melanoma," Int. J. Radiat. Oncol., Biol., Phys. **39**, 997–1010 (1997).
[26]P. L. Petti (private communication).
[27]W. Rasband (National Institute of Health, Bethesda, MD).
[28]MATLAB, *Image Processing Toolbox* (Math Works, Natick, MA, 1997).
[29]F. Mihara, K. L. Gupta, S. Murayama, N. Lee, J. B. Bond, and B. G. Haik, "MR imaging of malignant uveal melanoma—Role of pulse sequence and contrast agent," Am. J. Roentgenol. **157**, 1087–1092 (1991).
[30]L. Manfre, G. Fabbri, T. Avitabile, P. Biondi, A. Reibaldi, and G. Pero, "Mri and Intraocular Tamponade Media," Neuroradiology **35**, 359–361 (1993).
[31]J. M. Caudrelier, S. Vial, D. Gibon, C. Kulik, C. Fournier, B. Castelain, B. Coche-Dequeant, and J. Rousseau, "MRI definition of target volumes using fuzzy logic method for three-dimensional conformal radiation therapy," Int. J. Radiat. Oncol., Biol., Phys. **55**, 225–233 (2003).
[32]S. McCaffery, E. M. Simon, N. J. Fischbein, H. A. Rowley, A. Shimikawa, S. Lin, and J. M. O'Brien, "Three-dimensional high-resolution magnetic resonance imaging of ocular and orbital malignancies," Arch. Ophthalmol. (Chicago) **120**, 747–754 (2002).
[33]I. K. Daftari, P. L. Petti, J. M. O'Brien, and T. L. Phillips, in *4th Annual CyberKnife User's Meeting*, Half Moon Bay, California, 2005 (Half Moon Bay, CA, 2005).
[34]I. K. Daftari, P. L. Petti, D. C. Shrieve and T. L. Phillips, "Newer radiation modalities," Int. Ophthalmol. Clin. (to be published).